

Estimating Acceleration and Lane-Changing Dynamics from Next Generation Simulation Trajectory Data

Christian Thiemann, Martin Treiber, and Arne Kesting

The Next Generation Simulation (NGSIM) trajectory data sets provide longitudinal and lateral positional information for all vehicles in certain spatiotemporal regions. Velocity and acceleration information cannot be extracted directly because the noise in the NGSIM positional information is greatly increased by the necessary numerical differentiations. A smoothing algorithm is proposed for positions, velocities, and accelerations that can also be applied near the boundaries. The smoothing time interval is estimated on the basis of velocity time series and the variance of the processed acceleration time series. The velocity information obtained in this way is then applied to calculate the density function of the two-dimensional distribution of velocity and inverse distance and the density of the distribution corresponding to the “microscopic” fundamental diagram. It is also used to calculate the distributions of time gaps and times to collision, conditioned to several ranges of velocities and velocity differences. By simulating virtual stationary detectors, it is shown that the probability for critical values of the times to collision is greatly underestimated when estimated from single-vehicle data of stationary detectors. Finally, the lane-changing process is investigated, and a quantitative criterion is formulated for the duration of lane changes that is based on the trajectory density in normalized coordinates. There is a noisy but significant velocity advantage in favor of the targeted lane that decreases immediately before the change due to anticipatory accelerations.

FHWA originated Next Generation Simulation (NGSIM) to “improve the quality and performance of simulation tools, promote the use of simulation for research and applications, and achieve wider acceptance of validated simulation results” (1). As part of the program, a first data set was collected at the Berkeley Highway Laboratory (BHL) in Emeryville, California, by Cambridge Systematics and the California Center for Innovative Transportation at the University of California, Berkeley. BHL is part of I-80 on the east coast of the San Francisco Bay. Six cameras mounted on top of the 97-m Pacific Park Plaza tower recorded 4,733 vehicles on a road section approximately 900 m long in a 30-min period in December 2003. The result was published as a prototype data set. As part of the California Partners for Advanced Highways and Transit Program, the Institute of Trans-

portation Studies at University of California at Berkeley further enhanced the data-collection procedure (2), and in April 2005, another trajectory data set was recorded at the same location by using seven cameras and capturing a total of 5,648 vehicle trajectories in three 15-min intervals on a road section of approximately 500 m. This was later published as the I-80 data set. In June 2005, a data collection was made by using eight cameras on top of the 154-m 10 Universal City Plaza building, next to the Hollywood Freeway, US-101. On a road section of 640 m, 6,101 vehicle trajectories were recorded in three consecutive 15-min intervals. This data set was published as the US-101 data set. All data sets are freely available for download from the NGSIM website (www.ngsim.fhwa.dot.gov).

This amount of trajectory data is unique in the history of traffic research and provides a better basis for the validation and calibration of microscopic traffic models. Lu and Skabardonis examined the backward propagation speed of traffic shock waves by using the two later data sets (3). However, most recent attention focuses on the investigation of lane changes: Roess and Ulerio used the two later data sets to study some trends and sensitivities in weaving sections (4), especially lane changes. Zhang and Kovvali (5) and Goswami and Bham (6) investigated the gap acceptance behavior in lane-changing situation on freeways. By using the prototype and I-80 data sets, Toledo and Zohar investigated the duration of lane changes (7). Choudhury et al. calibrated a lane-changing model by using the I-80 data set and validated the model by using virtual loop detectors placed into the US-101 data (8). Leclercq et al. calibrated a model of the headway relaxation phenomenon observed in lane-changing situations by using the I-80 data set (9). Other studies have also used the NGSIM data (10–13).

In all these studies, the longitudinal and lateral position information of the trajectory data was used directly. There have been few investigations of the data regarding topics for which velocities and accelerations play a significant role, such as testing or calibrating car-following models (14) or lane-changing models or estimating fuel consumption (15). Since velocities and accelerations are derived quantities, the noise in the NGSIM positional information is greatly increased and a direct application is not possible.

This work proposes and motivates a smoothing method that allows the NGSIM data to be used for data analysis by using velocity or acceleration information. The velocities are used to calculate the density function of the two-dimensional distribution of velocity and inverse distance and the density of the distribution corresponding to a microscopic fundamental diagram. The data also are used to calculate the distributions of time gaps and times to collision, conditioned to several ranges of velocities and velocity differences. The measurements of spatial quantities by virtual loop detectors are compared to the real values determined from the trajectory data. A

C. Thiemann, Department for Nonlinear Dynamics, Max Planck Institute for Dynamics and Self-Organization, Bunsenstr. 10, D-37073 Göttingen, Germany. M. Treiber and A. Kesting, Institute for Transport and Economics, Technische Universität Dresden, Andreas-Schubert-Str. 23, D-01062 Dresden, Germany. Corresponding author: A. Kesting, kesting@wwi.tu-dresden.de.

Transportation Research Record: Journal of the Transportation Research Board, No. 2088, Transportation Research Board of the National Academies, Washington, D.C., 2008, pp. 90–101.
DOI: 10.3141/2088-10

method is proposed to determine the lane-change duration from the NGSIM data.

EXTRACTING VELOCITY AND ACCELERATION INFORMATION

Trajectory data available for download appear to be unfiltered and also exhibit some noise artifacts. All data sets include velocity and acceleration. However, they appear to have been numerically derived from the tracked vehicle positions without any processing. Figure 1 visualizes the problems of the data. In the prototype data set, two-thirds of all accelerations are beyond $\pm 3 \text{ m/s}^2$ (which are then reported as $\pm 3 \text{ m/s}^2$ in the data file). The example trajectory shows that the driver is allegedly changing between hard acceleration and hard deceleration several times a second, which is unrealistic. In the I-80 and US-101 data sets, the acceleration distributions are more realistic—although approximately 10% are beyond $\pm 3 \text{ m/s}^2$. However, in the later data sets, the velocity distributions are very spiky, that is, velocities tend to snap to certain values. The velocities of an example trajectory exhibit an unrealistic behavior: taken as real, they would mean that drivers do not smoothly brake or accelerate but rather use the gas and brake pedals only occasionally although press hard, to quickly change between preferred velocities. Also, to produce the spikes in the velocity distribution, all drivers must happen to like the same velocities. This is unrealistic and therefore the velocity spikes must be an artifact of the measurement method. One may credit the velocity spikes to discretization errors (time and space are discretized; thus velocity can take only certain discrete values as well), but two observations object to that. First, the spikes are not delta peaks; other velocities still appear. Second, given the time discretization $dt = 1/10 \text{ s}$ and the approximate distance between the velocity spikes $dv = 0.7 \text{ m/s}$, this would mean that the spatial accuracy of the measurement method is just 7 m, which is obviously not the case. It is suspected therefore that the velocity spikes are introduced by some data postprocessing.

To correct those artifacts, a symmetric exponential moving average filter (sEMA) is applied to all trajectories before any further data analysis.

Let $x_\alpha(t_i)$ denote the measured position of vehicle α at time t_i , where $i = 1 \dots N_\alpha$ and N_α denotes the number of data points of the trajectory. The smoothing kernel is given by $g(t) = \exp(-|t|/T)$, where T is the smoothing width. Since the data points are equidistant in time with interval dt , the smoothing operation can be formulated by using data point indices instead of times. The smoothed positions $\bar{x}_\alpha(t_i)$ are given by

$$\bar{x}_\alpha(t_i) = \frac{1}{Z} \sum_{k=i-D}^{i+D} x_\alpha(t_k) e^{-|i-k|/\Delta}$$

where

$$Z = \sum_{k=i-D}^{i+D} e^{-|i-k|/\Delta} \quad (1)$$

The smoothing width Δ is given by

$$\frac{T}{dt}$$

and transparently handles the different time intervals in the data sets. (The prototype data set uses $dt = 1/5 \text{ s}$, whereas the later two use $dt = 1/10 \text{ s}$.) The same real-time smoothing width T can be used for all data sets, and

$$\Delta = \frac{T}{dt}$$

will be the corresponding smoothing width measured in data points for the specific data set. The smoothing window width $D = \min\{3\Delta, i-1, N_\alpha - i\}$ is chosen to be three times the smoothing kernel width for any data point that is not closer than D data points to either trajectory boundary. For the points near the boundaries, the smoothing width is decreased to ensure that the smoothing width is always symmetric.

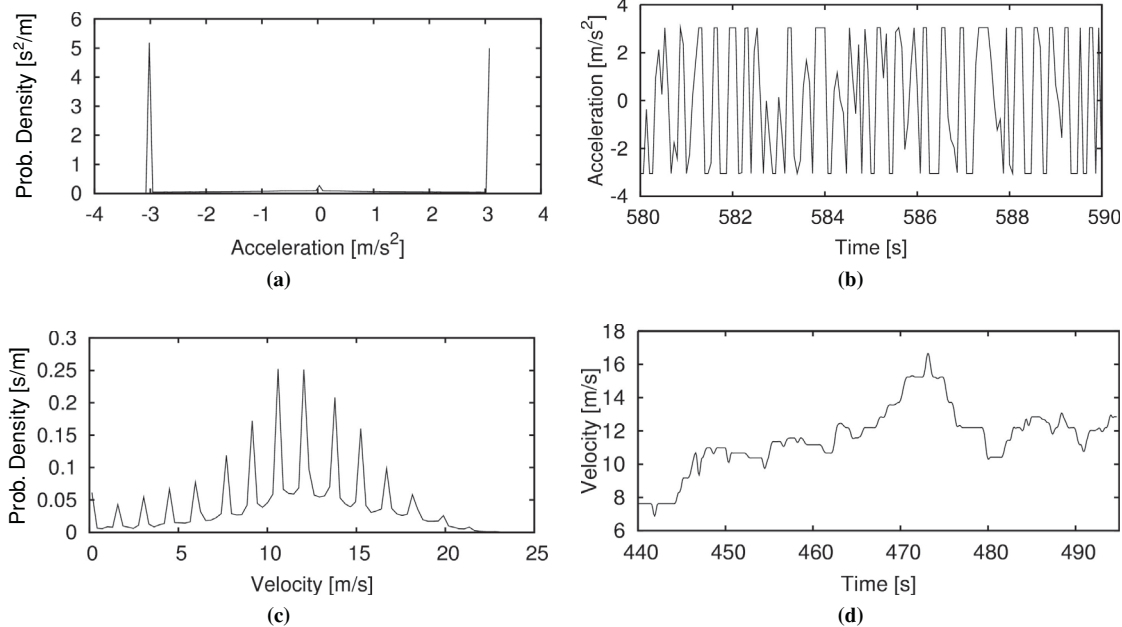


FIGURE 1 Problems of original, unsmoothed data: (a) acceleration distribution, (b) example trajectory excerpt, (c) velocity distribution of 7:50–8:05 a.m. data file of US-101 data set, and (d) example trajectory (velocity).

It may be objected that other filters would work as well or even better—for example, the Kalman filter or a simple moving average. A moving average filter, which would correspond to Equation 1 with the exponentials removed, has noncontinuous filter boundaries, that is, with moving, the filter data points suddenly slip into the smoothing window with full weight or suddenly drop out. This can cause smoothing artifacts that are prevented by using a weighted moving average, where the weight decreases with increasing distance from the smoothing window center. This way, data points will be smoothly incorporated into the smoothing window and fall out smoothly as well. It was found that an exponential weight function leads to better results than a Gaussian filter, and so sEMA was chosen. The Kalman filter needs a simple traffic model and thus introduces some significant assumptions into the smoothing process. Also, the Kalman filter has more parameters, whereas the sEMA method has only one parameter, T , and does not introduce complicated assumptions.

Another possible filter would be not to use some moving kernel filter but rather to increase the step size from dt to $n \cdot dt$ in calculation of the velocities and accelerations, that is,

$$\frac{v(t) = (x(t + n \cdot dt) - x(t - n \cdot dt))}{(2 \cdot n \cdot dt)}$$

It can be shown that this filter is equal to a simple moving average for the velocities and a composition of two moving averages for the accelerations (which simplifies to a triangular moving average when boundary regions are neglected). This filter is a faster but somewhat worse alternative to the proposed method.

Having defined the fundamental smoothing mechanism, there are still two open questions. First, the order of differentiations and smoothing operations needs to be defined. Second, a smoothing width T must be found.

There are three possible answers to the first question: (a) smooth positions, then differentiate to velocities and accelerations; (b) first differentiate to velocities and accelerations and then smooth all three variables; and (c) smooth positions, differentiate to velocities, smooth velocities, differentiate to accelerations, and smooth accelerations. For $D + 2 \leq i \leq N_\alpha - D - 1$, the smoothing (1) commutes with the differentiation, and all these methods are equivalent. In view of the short trajectories, however, the points closer to the boundary cannot be neglected.

The first method is problematic, as can be seen by the following reasoning. Consider an artificial trajectory with constant acceleration:

$$x(t_i) = \frac{1}{2} a t_i^2$$

Any symmetric smoothing kernel will overestimate the position and produce a trajectory $\bar{x}(t_i) > x(t_i)$. Sufficiently far away from the boundaries, the smoothing window width D is constant and the smoothed trajectory

$$\bar{x}(t_i) = x(t_i) + \frac{1}{2} a \sigma_g^2$$

has a constant error proportional to the variance σ_g^2 of the smoothing kernel. Near the boundaries, however, D and σ_g will become smaller and vanish for $i = 1$ and $i = N$, which results in $\bar{x}(t_1) = x(t_1)$ and $\bar{x}(t_N) = x(t_N)$. Thus, the offset of the smoothed positions becomes smaller when approaching the boundaries, which of course induces a bias to the velocity. Moreover, if the smoothing kernel does not completely vanish at the smoothing window borders, the transition between constant offset and decreasing offset will not be continu-

ously differentiable, inducing a jump in velocity and thus an even larger jump in the acceleration. Therefore, use of this smoothing method is discouraged.

To choose the second or third smoothing method, artificial benchmark trajectories have been generated and white noise has been added to the positions. The second method—first the differentiation to velocities and accelerations and then the smoothing of the three variables—turned out to better reproduce the original trajectories, and so this method was used.

This left the difficult question of which smoothing width T to use. There is no generic recipe, but some hints help make this decision not completely arbitrary. First, the most vivid trajectories—those with a large velocity range—were extracted from each data set, and the variance of the accelerations, σ_a^2 , were compared for different smoothing widths (Figure 1a). For $T \rightarrow \infty$, the acceleration variance of the smoothed trajectory would vanish, but the variance that is caused by the noise vanishes much faster than the one caused by the real acceleration data. Thus, with finite T the noise is smoothed out very quickly, leading to a fast drop in $\sigma_a^2(T)$ at small T . For larger T , $\sigma_a^2(T)$ appears to be nearly constant. Keeping in mind that the real acceleration data are smoothed a bit as well, the plot suggests a smoothing width of about 4 s.

However, this value is a suggestion for the acceleration smoothing width only. It is not necessary to use such large smoothing widths for the positions and velocities. Let $X_\alpha(t_i)$ be a random variable describing the positions of vehicle α with expectation value $\bar{x}_\alpha(t_i)$ and variance $\sigma_x^2(t_i)$. The measured trajectory $x_\alpha(t_i)$ is a realization of $X_\alpha(t_i)$ and, assuming unbiased noise, the real trajectory is equal to $\bar{x}_\alpha(t_i)$. Two new random variables describe the velocities and accelerations of vehicle α in terms of symmetric difference quotients:

$$V_\alpha(t_i) = \frac{X_\alpha(t_i + dt) - X_\alpha(t_i - dt)}{2dt} \quad (2)$$

$$A_\alpha(t_i) = \frac{X_\alpha(t_i + dt) - 2X_\alpha(t_i) + X_\alpha(t_i - dt)}{dt^2} \quad (3)$$

Since this is a linear combination of random variables, the expectation values of $V_\alpha(t_i)$ and $A_\alpha(t_i)$ will be the first and second derivative of $\bar{x}_\alpha(t_i)$, respectively (the real velocities and the real accelerations). Assuming uncorrelated noise, the variances of $V_\alpha(t_i)$ and $A_\alpha(t_i)$ are given by

$$\sigma_v^2(t_i) = \frac{\sigma_x^2(t_i)}{2dt^2}$$

and

$$\sigma_a^2(t_i) = \frac{6\sigma_x^2(t_i)}{dt^4} \quad (4)$$

Thus, the noise will be strongly amplified by the differentiation, and therefore the velocities must be weaker smoothed than the acceleration and the positions weaker than the velocities.

Figures 2b and 2c, the lateral positions and longitudinal velocities and accelerations of a sample trajectory of the US-101 data set are plotted as original data and for different smoothing widths. The position smoothing width T_x is critical, because the lane change duration is quite sensitive to it. As visible in the plot, a large T_x will significantly smear out the trajectory leading to larger lane-change durations. To resolve the issue with the preferred velocities, the smoothing of the velocities should be strong enough so that the smoothed velocities

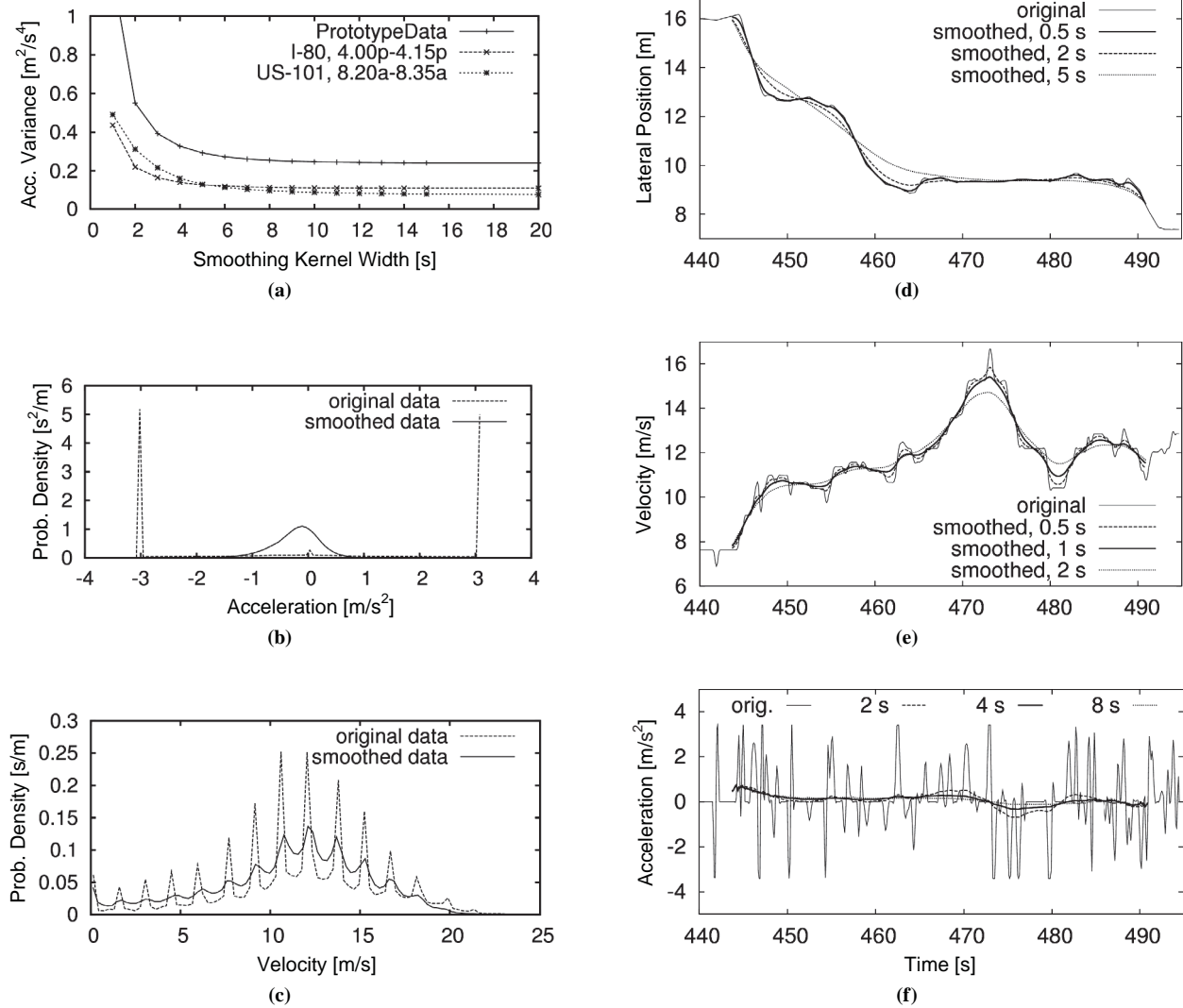


FIGURE 2 Effects of applied trajectory smoothing: (a) dependency of acceleration variances on smoothing kernel width, (b) acceleration distribution in prototype data set, and (c) velocity distribution in 7:50–8:05 a.m. data file of US-101 data set. Sample trajectory of US-101 data set with different applied smoothing kernel widths: (d) lateral position, (e) longitudinal velocity, and (f) acceleration.

no longer follow the trends of this semiquantization. However, the smoothing should be as weak as possible because the velocity smoothing width also quantitatively influences some results. The smoothing times

$$T_x = 0.5 \text{ s}$$

$$T_y = 1 \text{ s}$$

and

$$T_a = 4 \text{ s} \quad (5)$$

were chosen.

The effects of this smoothing on the acceleration distribution of the prototype data set and the velocity distribution of the two later data sets can be seen in Figures 2d through 2f.

RESULTS

Most empirical traffic state data are gathered by stationary loop detectors that can measure quantities at different times but at a single location only. These measurement devices are therefore capable of measuring temporal quantities but not spatial quantities. However, since both spatial and temporal quantities are important in traffic science, it is common practice to derive the spatial quantities from temporal measurements by using some conservation assumptions (e.g., constant vehicle velocities within a certain period). Modern trajectory data like the NGSIM recordings provide enough data to enable a validation of these practices. The following describes the analysis process to obtain spatial information from temporal data, and vice versa, and its accuracy is checked for three examples: the microscopic fundamental diagram and the distributions of the time gaps and times to collision. Later, lane changes in the NGSIM data are investigated. All analysis uses the smoothed data sets obtained by the smoothing

method introduced and motivated earlier; all references to any NGSIM data set are to be understood as references to the smoothed data sets.

Spatial and Temporal Quantities from Momentary and Stationary Measurements

The two measurement types to be compared are the traditional stationary loop detector, which is singular in space but continuous in time, and an aerial photograph, which is continuous in space but singular in time. The basic idea of the analysis is to place virtual loop detectors into the trajectory data. These would correspond to lines parallel to the time axis in a space–time plot, whereas lines parallel to the space axis correspond to momentary snapshots (virtual photographs) of the measurement area (Figure 3). Wherever those lines intersect, both stationary and momentary measurements are available for comparison. To maximize the amount of data available for comparison, the following algorithm was applied to the data: For every 10th data point of each trajectory, the spatial leader and the temporal leader are determined. The spatial leader $\alpha - 1$ is the vehicle currently driving ahead of the vehicle α , and the temporal leader is the vehicle that most recently passed the actual position of vehicle α . (For simplicity, the temporal leader is denoted by $\alpha - 1$ as well.) The first information is available only to momentary measurements, whereas the second is available only to stationary measurements.

Assuming double loop detectors for the stationary measurement, the passage times t_α and $t_{\alpha-1}$ of vehicle α and $\alpha - 1$ and their velocities at the time of passing the detector are available: $v_\alpha(t_\alpha)$, $v_{\alpha-1}(t_{\alpha-1})$. Furthermore, the length of the leading vehicle $l_{\alpha-1}$ is known, as are the positions (front bumper) at the time of passing the detector: $x_\alpha(t_\alpha) = x_{\alpha-1}(t_{\alpha-1})$.

From the momentary measurement at time t_α one obtains the positions of the two vehicles, $x_\alpha(t_\alpha)$ and $x_{\alpha-1}(t_\alpha)$, as well as the length of the leading vehicle $l_{\alpha-1}$. Assuming that two consecutive photographs are taken, one can also determine the velocities $v_\alpha(t_\alpha)$ and $v_{\alpha-1}(t_\alpha)$. From this momentary measurement, the following spatial quantities can be calculated:

$$\text{spatial gap } s_\alpha(t_\alpha) = x_{\alpha-1}(t_\alpha) - x_\alpha(t_\alpha) - l_{\alpha-1} \quad (6)$$

$$\text{approaching rate } \Delta v_\alpha(t_\alpha) = v_\alpha(t_\alpha) - v_{\alpha-1}(t_\alpha) \quad (7)$$

Assuming constant velocities within the time interval $\Delta t_\alpha = t_\alpha - t_{\alpha-1}$, one can estimate the same quantities from data collected by a stationary detector:

$$s_\alpha^{\text{est}}(t_\alpha) = v_{\alpha-1}(t_{\alpha-1}) \cdot \Delta t_\alpha - l_{\alpha-1} \quad (8)$$

$$\Delta v_\alpha^{\text{est}}(t_\alpha) = v_\alpha(t_\alpha) - v_{\alpha-1}(t_{\alpha-1}) \quad (9)$$

Furthermore, the time gap T defined by the gap related to the actual velocity, $\frac{s}{v}$, is a crucial quantity for the safety and capacity of traffic flow. From the time interval between two vehicles passing the stationary detector, $\Delta t_\alpha = t_\alpha - t_{\alpha-1}$, one can estimate the time gap while passing the detector:

$$T_\alpha^{\text{est-pt}}(t_\alpha) = \Delta t_\alpha - \frac{l_{\alpha-1}}{v_{\alpha-1}(t_{\alpha-1})} \quad (10)$$

This definition assumes constant velocity of the leading vehicle in the time interval Δt_α . The real time gap, however, would be obtained by measuring the time where the rear bumper of the leading vehicle passed the detector:

$$T_\alpha(t_\alpha) = t_\alpha - t'$$

with t' such that

$$x_{\alpha-1}(t') - l_{\alpha-1} = x_\alpha(t_\alpha) \quad (11)$$

Both quantities are illustrated in Figure 3b. Alternatively, one can estimate the time gap $T_\alpha^{\text{est,mom}}$ from data collected by a momentary detector, again assuming constant velocities of the vehicles:

$$T_\alpha^{\text{est,mom}}(t_\alpha) = \frac{s_\alpha(t_\alpha)}{v_{\alpha-1}(t_\alpha)} \quad (12)$$

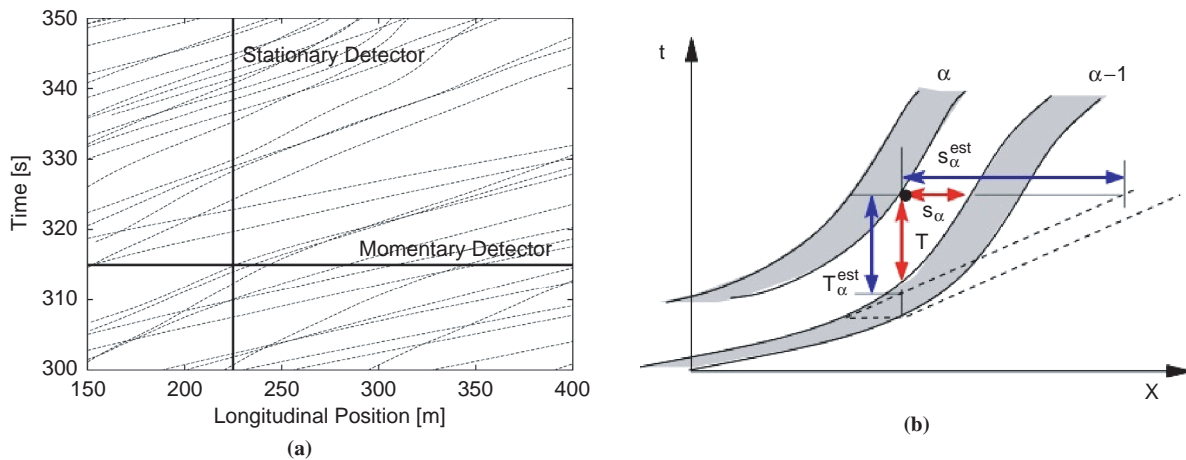


FIGURE 3 (a) Virtual detectors in space–time plot; stationary detectors (loop detectors) correspond to lines parallel to time axis and momentary detectors (aerial photographs) correspond to lines parallel to the space axis. (b) Illustration of time gap $T_\alpha^{\text{est-pt}}$ according to Equation 10, assuming constant velocities and real time gap T . ($T_\alpha^{\text{est-pt}}$ is estimate from stationary measurement, whereas $T_\alpha^{\text{est,mom}}$ as defined in Equation 12 is estimate from momentary measurement.)

Data Preparation

In total, 184,171 data points in the prototype data set and 722,904 in the two other data sets were investigated. Data points that were too close to the downstream boundary needed to be discarded since no spatial leader could be identified. Furthermore, data points that were closer than 3 s to a lane-changing event were ignored, leaving 146,213 data points from the prototype data set and 675,660 from the I-80 and US-101 data sets.

Because of tracking or vehicle dimension detection errors, some spatial and time gaps are negative or very small. A small spatial gap s_α leads to a very large inverse time to collision τ_α , which would dominate any higher-order moments of the τ_α distribution. Thus, the data were filtered such that $s_\alpha \geq 1$ m and $T_\alpha \geq 0.1$ s hold for every data point. This filter removed a further 3,070 data points (2.1%) from the prototype data set extract and 11,755 (1.7%) from the extract of the two later data sets.

Microscopic Fundamental Diagram and Stopped Traffic

From the described spatiotemporal measurements, one can derive the inverse of the space headway, $(\Delta x_\alpha)^{-1} = (x_{\alpha-1} - x_\alpha)^{-1}$, and the inverse of the time headway, $(\Delta t_\alpha)^{-1}$. These quantities are more intuitively described as microscopic density and microscopic flow, respectively, and are referred to by these names throughout this section. For the prototype data set and the combined other two data sets, the distribution of velocity and microscopic density are plotted in Figures 4a and 4b. The prototype data set mainly features free traffic and some

bound traffic, whereas the two later data sets feature only bound and jammed traffic. By plotting microscopic flow versus microscopic density for all three data sets, the fundamental diagram was plotted (Figure 4c). The free flow part of the diagram is completely provided by the prototype data set, and the bound and jammed part is almost completely provided by the I-80 and US-101 data sets. Notice that in contrast to the prototype data set, the later two sets exhibit stripes corresponding to the preferred velocities as seen in Figure 1, which are much more prominent when applying the same procedure to the original, unsmoothed data.

From the rich amount of data in the jammed traffic regime, it is also possible to determine the average headway of standing vehicles. All data points with velocities $v_\alpha < 0.05$ m/s were extracted, and the distribution of Δx_α is plotted in Figure 4f. The mode is at approximately 7 m for cars and 8 m for trucks (with a smaller second peak at 14 m). However, the distribution is right-skewed, so that the mean values are a little higher: 8.3 m for cars and 9.7 m for trucks. Note that for principal reasons, this distribution cannot be obtained from stationary detector data.

Time Gap Distribution

Consider now the time gaps as defined in Equations 10, 11, and 12. Figure 5 plots the time gap distribution in three different traffic regimes: free traffic ($v > 22$ m/s), jammed traffic ($v < 15$ m/s), and bound traffic (intermediate velocities). Furthermore, in every plot, the real time gap T_α defined by Equation 11 as obtained from the trajectories is compared to the estimated time gap from momentary measurement $T_\alpha^{\text{est,mom}}$ (Equation 12). First note the remarkable

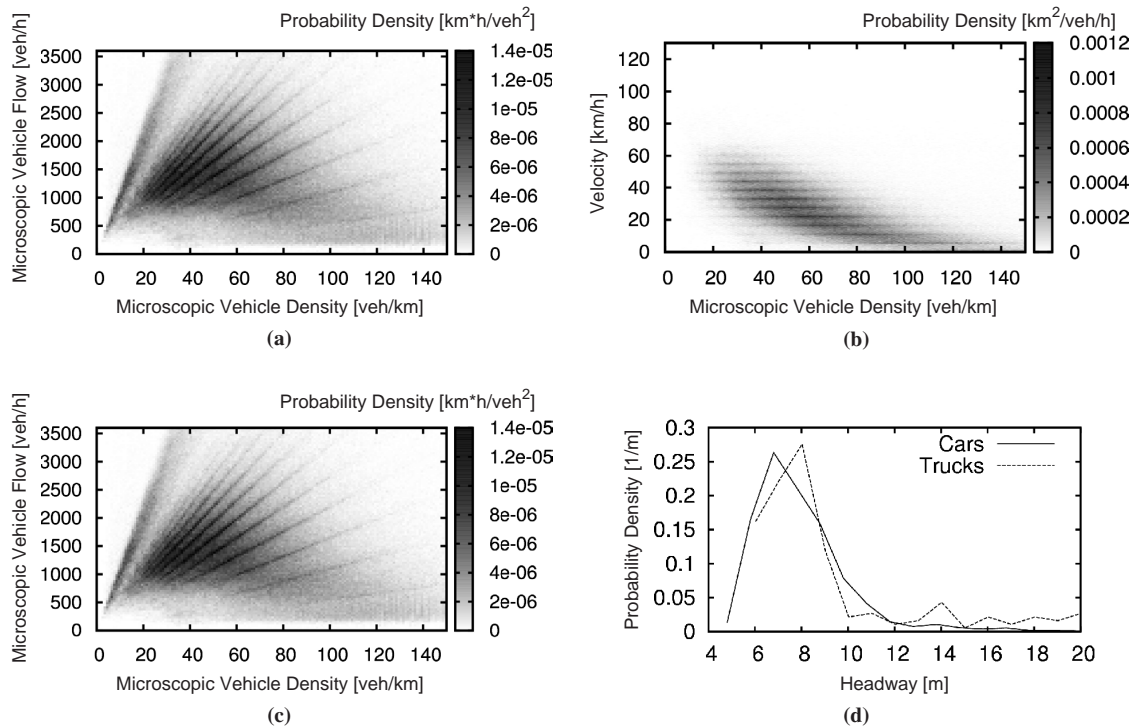


FIGURE 4 Probability density of two-dimensional distribution of microscopic density $(x_{\alpha-1} - x_\alpha)^{-1}$ versus velocity v_α in (a) prototype data set (upper left) and (b) two later I-80 and US-101 data sets. Probability density of (c) microscopic density versus microscopic flow T_α^{-1} and of (d) distribution of headways $x_{\alpha-1} - x_\alpha$ in stopped traffic ($v_\alpha < 0.05$ m/s); mean value is 8.3 m for cars and 0.0 m for trucks, respectively.

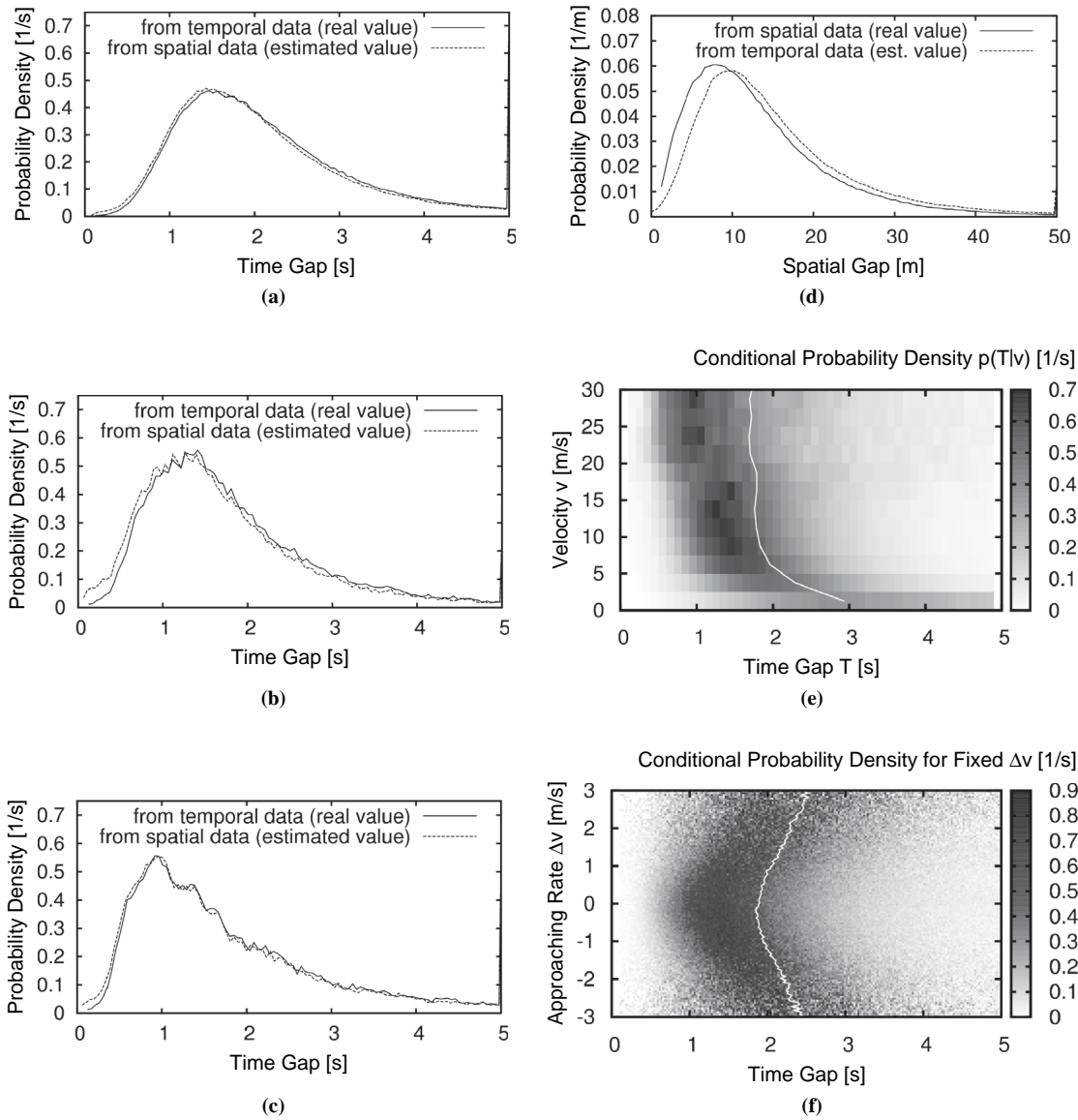


FIGURE 5 Distributions: (a) time gap T_{α} in jammed traffic, (b) time gap T_{α} in bound traffic, (c) time gap T_{α} in free traffic, (d) spatial gap s_{α} in jammed traffic, (e) distribution of time gap for different given velocities v_{α} , and (f) distribution of time gap for different given approaching rates Δv_{α} . White lines show the mean value for each row of plot, that is, mean of time gap for different values of v or Δv .

indifference of the distributions to the measurement method. For comparison, the spatial gap distribution in jammed traffic was plotted (Figure 5b), which the stationary measurements shifts to larger values. In the other two traffic regimes the spatial gap distributions agree very well.

The mode of the time gap distribution shifts from approximately 1.5 s in jammed traffic to 1 s in free traffic. This effect is shown in Figure 5d. The mean time gap is 2.6 s in jammed traffic, 1.9 s in bound traffic, and 2.0 s in free traffic. Figure 5f shows another dependency of the time gap: although data become sparse toward larger values, there is a significant tendency toward larger time gaps if the velocity difference to the leading vehicle is large (regardless of whether approaching the vehicle or falling behind).

In addition to comparing time gaps measured by stationary detectors to time gaps measured by momentary detectors, there are other

ways to determine the time gap with a stationary detector. The real time gap is the time between the leader's rear bumper and the following front bumper passing the detector (Equation 11). However, if detectors produce only passage times and vehicle lengths and velocities, one needs to estimate the time gap from the passage by assuming constant velocity of the leader vehicle while passing the detector (Equation 10). This error is very small in most cases: only 10% of the sample data points had an error in the estimate from passage times $T_{\alpha}^{est,pt}$ that exceeded 10% of the real time gap T_{α} .

Time to Collision

Another relevant quantity is the time to collision (TTC), which serves as a safety measure for traffic situations because it states the time

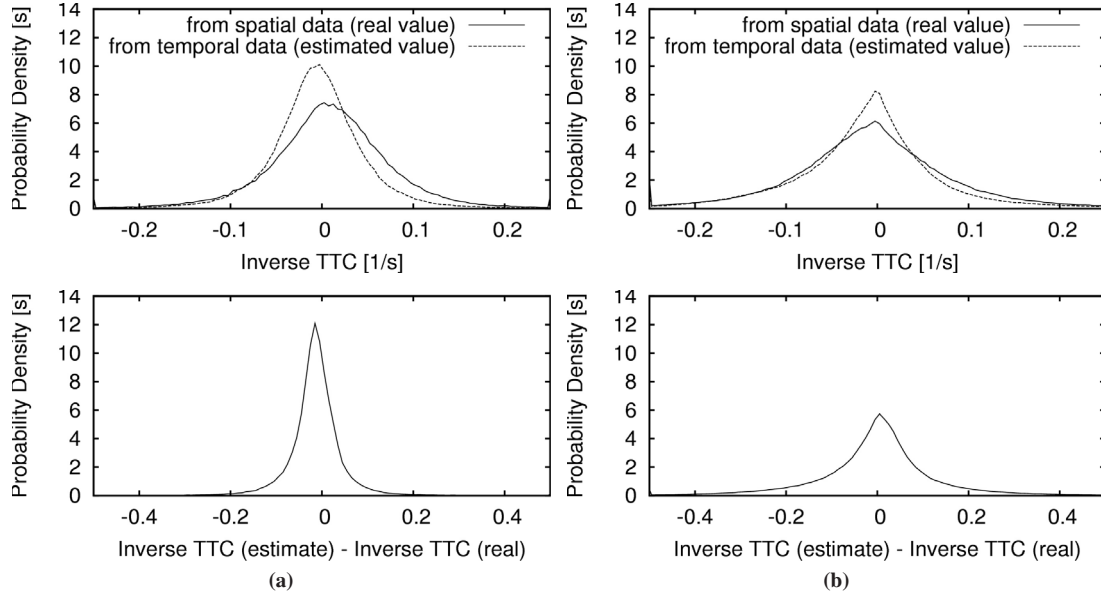


FIGURE 6 Distribution of inverse time to collision τ_α^{-1} : (a) in prototype data set and (b) in two later data sets compared with estimated time to collision $(\tau_\alpha^{\text{est}})^{-1}$ obtained from stationary measurements. Upper figures show both distributions, and lower figures show distributions of measurement errors $\Delta\tau_\alpha^{-1} = (\tau_\alpha^{\text{est}})^{-1} - \tau_\alpha^{-1}$.

left until the vehicle will crash into its leader unless at least one of the drivers changes speed (16, 17). The TTC as a spatial quantity is defined by Equations 6 and 7 as

$$\tau_\alpha(t_\alpha) = \frac{s_\alpha(t_\alpha)}{\Delta v_\alpha(t_\alpha)} \quad (13)$$

The TTC can also be estimated from stationary (temporal) measurements in Equations 8 and 9:

$$\tau_\alpha^{\text{est}}(t_\alpha) = \frac{s_\alpha^{\text{est}}(t_\alpha)}{v_\alpha(t_\alpha) - v_{\alpha-1}(t_{\alpha-1})} \quad (14)$$

The impact of the constant-velocity assumption used to derive the TTC τ_α^{est} from stationary measurements is investigated next. Since the TTC diverges for $\Delta v_\alpha = 0$, it is more convenient to discuss the TTC in terms of its inverse,

$$\tau_\alpha^{-1} = \frac{\Delta v_\alpha}{s_\alpha}$$

Figures 6a and 6c plot the distribution of the inverse TTC in the prototype data set, and Figures 6b and 6d plot the distribution in the two later data sets. In contrast to the spatial and time gap distributions, the inverse TTC distribution differs significantly between the two measurement methods. The inverse TTC is sensitive to errors in the spatial gap, especially when the gap is small. Therefore, inverse TTC values with absolute value larger than 1 were ignored in computing statistical properties of the distributions. In this way, 0.59% of all data points were ignored.

The mean of the absolute error $\Delta\tau_\alpha^{-1} := (\tau_\alpha^{\text{est}})^{-1} - \tau_\alpha^{-1}$ is 0.00098 in the prototype data set and -0.0134 in the two later data sets. The same can be observed when splitting the data from all data sets into traffic regimes. The mean error is 0.000045 in jammed traffic, -0.0067 in bound traffic, and -0.0122 in free traffic. The variance of the errors is strongest in jammed traffic (0.0236), whereas it is 0.00388 in bound traffic and is 0.00225 in free traffic. Statistical properties of the inverse TTC distributions have been collected into Table 1. In the mean, variance, and skewness columns, the top value is obtained from momentary measurements (the real value), whereas the bottom

TABLE 1 Statistical Properties of Inverse TTC Distributions

Data Set	Mean	Variance	Skewness	Sign Change (%)
Prototype	0.00874006	0.00706569	-0.264358	19.2402
	-0.00462994	0.00422629	0.16407	7.63705
I-80-US-101	-0.00640645	0.0122408	0.0109132	23.0413
	-0.00542511	0.0120666	1.58624	21.3802
Jammed traffic	-0.00637853	0.0124101	-0.000798933	23.6459
	-0.00633317	0.0121906	1.54999	21.1149
Bound traffic	0.00624585	0.00699072	-0.204996	15.0853
	-0.000502914	0.00348709	0.798759	10.7964
Free traffic	0.0126101	0.00483055	0.179115	16.6644
	0.000389615	0.00260696	0.459587	5.58995

value is obtained from stationary measurements (the estimated value). In the sign change column, the top value states the amount of data points for which the stationary measurement determines a positive time-to-collision whereas the momentary measurement determines a negative value. The bottom value gives the amount of data points for which the sign change is the other way around. The jammed, bound, and free traffic data sets are combined from the prototype and the two later NGSIM data sets. A data point was assigned to jammed traffic if the vehicle's velocity was below 15 m/s, to free traffic if $v_\alpha > 22.2$ m/s, and to bound traffic otherwise. The skewness is consistently shifted toward higher values by the stationary measurement. This is visible in the plots as well.

In view of the application of the TTC as a safety measure, it is critical that stationary measurements consistently decrease the probability of measuring a large positive inverse-time-to-collision value that corresponds to a small positive τ_α , indicating a dangerous traffic situation. For example, in free traffic (Figure 7), the fraction of positive TTC values below 5 s (0.8% of the data points) that is considered critical (16, 17) is underestimated by the stationary measurement by about a factor of two. Thus, stationary measurements tend to euphemize the danger of collision.

Lane Changes

In addition to the ability to compare stationary and momentary measurements, the NGSIM trajectory data sets provide a good basis to investigate lane changes. To determine the lane change duration, all lane changes in the NGSIM data were collected. However, the processed video data supplied with the NGSIM data sets show that sometimes the tracking algorithm accidentally misplaced a

vehicle across the lane boundary and back after a few time steps. Also, sometimes drivers aborted a lane change or quickly crossed two lanes. To examine only real and normal single-lane lane changes, all lane changes were filtered out that were closer than a certain threshold τ_{th} to another lane change, chosen to be $\tau_{th} = 5$ s. Also sorted out were all lane changes that did not involve one of the four left-most lanes, to reduce the effect of the on and off ramps on the lane change analysis.

With $\lambda_\alpha(t)$ denoting the lane used by vehicle α at time t , a lane-changing event occurs at time t_{lc} if $\lambda_\alpha(t_{lc}) \neq \lambda_\alpha(t_{lc} + t)$ (where t is the time interval between two consecutive data points of a trajectory). For each lane-changing event, a 20-s environment of the trajectory with time, longitudinal, and lateral position relative to the lane-changing event was extracted:

$$\text{relative time } \tau = t - t_{lc} \tag{15}$$

$$\text{relative longitudinal position } \xi_\alpha(\tau) = x_\alpha(\tau + t_{lc}) - x_\alpha(t_{lc}) \tag{16}$$

$$\text{relative lateral position } \eta_\alpha(\tau) = y_\alpha(\tau + t_{lc}) - y_\alpha(t_{lc}) \tag{17}$$

Thus a plot can be produced of the conditional probability density $p(\eta|\tau)$ that a vehicle is at a relative lateral position η at a certain time τ relative to the lane-changing event time (Figure 8a). From this, the lane-change duration can be roughly estimated at approximately 5 to 6 s by looking at the curvature of the two mode values $\hat{\eta}_+(\tau) = \text{argmax}_{\eta>0} \{p(\eta|\tau)\}$ and $\hat{\eta}_-(\tau) = \text{argmax}_{\eta<0} \{p(\eta|\tau)\}$. This procedure is similar to the approach by Toledo and Zohar (7), in which the lane-change start and end times of each trajectory were determined by looking at the curvature of the lateral position $y_\alpha(t)$. However, finding the correct point in the curvature may be somewhat

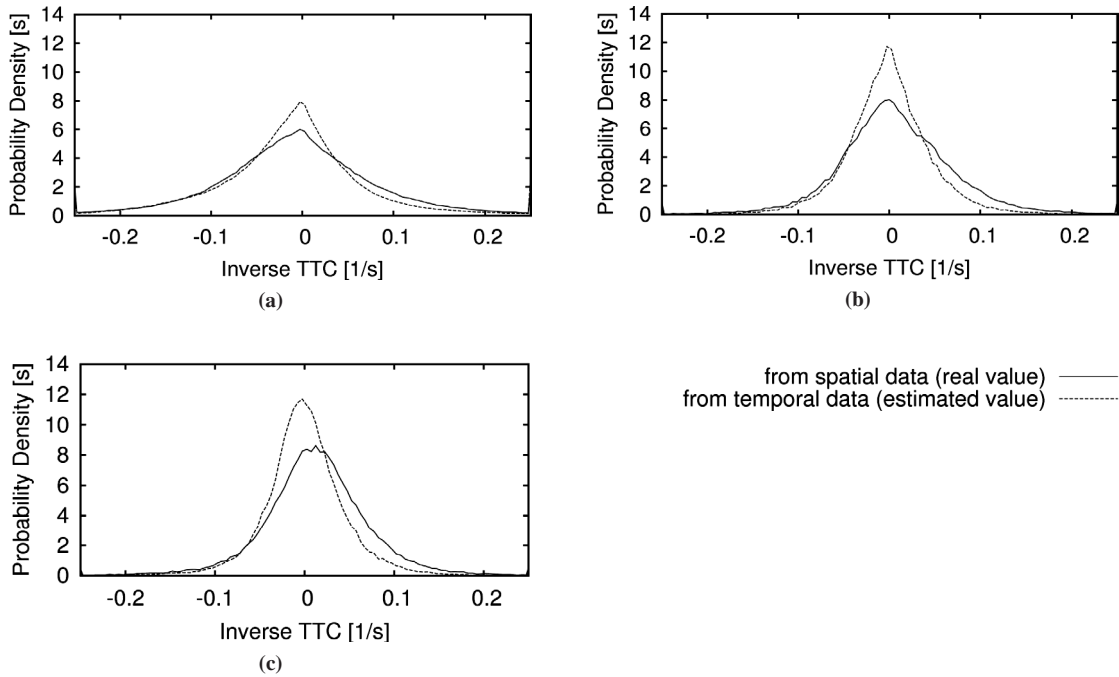


FIGURE 7 Distributions of inverse time to collision τ_α^{-1} of all data sets compared to estimated time to collision $(\tau_\alpha^{est})^{-1}$ obtained from stationary measurements: (a) jammed traffic, (b) bound traffic, and (c) free traffic.

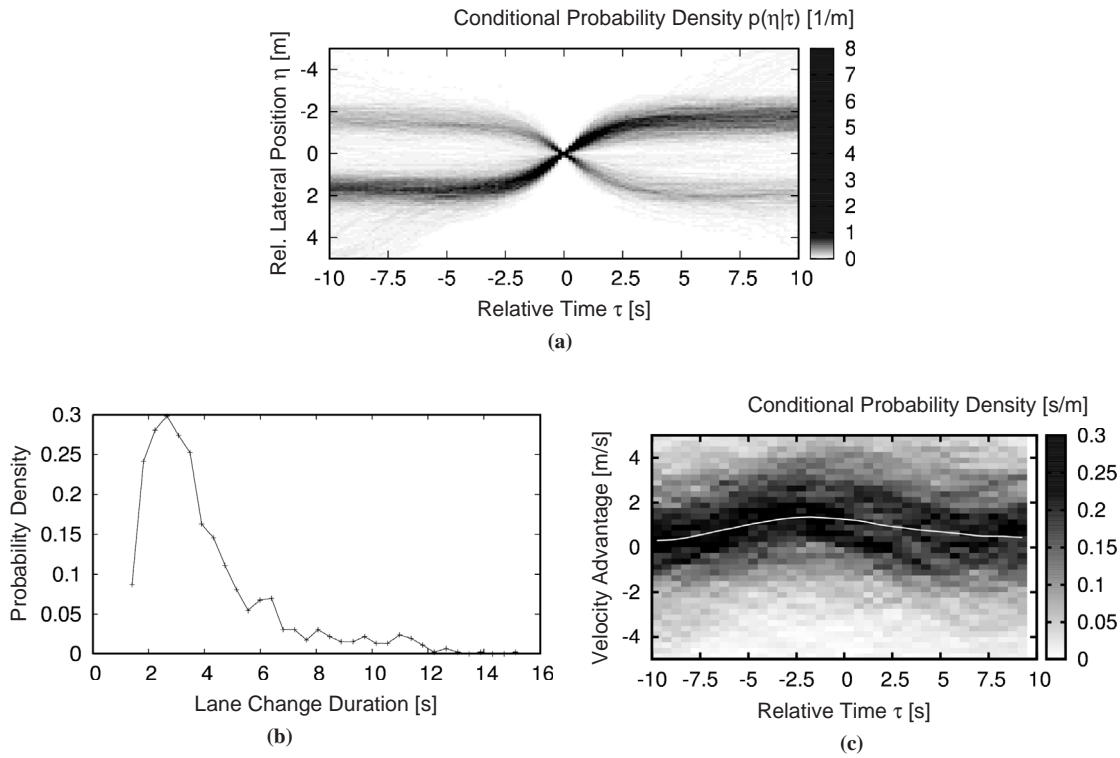


FIGURE 8 Lane changes: (a) conditional probability $p(\eta|\tau)$ of finding vehicle on lateral position η relative to lane boundary at given time τ relative to lane-changing event time, (b) distribution of lane-change durations T_{lc} according to Equation 20; mean lane-change duration is $\bar{T}_{lc} = (4.01 \pm 2.31)$ s, and (c) conditional probability density of velocity difference between leader on destination lane and leader on source lane for fixed times relative to lane-changing event (white line shows mean value).

arbitrary, and thus the following considers a more well-defined way to measure a lower bound of the lane-change duration.

The NGSIM vehicle detection algorithm detects not only the vehicle position but also its length l_α and width w_α . Since the lane assignment algorithm works such that each data point is placed into the lane in which its midpoint front-bumper position (x_α, y_α) lies, it is possible to determine the time at which a lane-changing vehicle first intruded into the destination lane and the time at which it completely left the source lane. Given the lane-changing event time t_{lc} and the relative time and position as defined in Equations 15 through 17, the relative start time τ_s and end time τ_e of the lane change may be defined as follows (a higher lane index λ_α corresponds to a larger lateral position η_α):

$$\tau_s = \begin{cases} \max \left\{ \begin{array}{l} \tau | \tau < 0 \text{ and } \eta_\alpha(\tau) + w_\alpha/2 < 0 \\ \tau | \lambda_\alpha(t_{lc}) < \lambda_\alpha(t_{lc} + \Delta t) \end{array} \right. & \text{if } \lambda_\alpha(t_{lc}) < \lambda_\alpha(t_{lc} + \Delta t) \\ \max \{ \tau | \tau < 0 \text{ and } \eta_\alpha(\tau) - w_\alpha/2 > 0 \} & \text{otherwise} \end{cases} \quad (18)$$

$$\tau_e = \begin{cases} \min \left\{ \begin{array}{l} \tau | \tau > 0 \text{ and } \eta_\alpha(\tau) - w_\alpha/2 > 0 \\ \tau | \lambda_\alpha(t_{lc}) < \lambda_\alpha(t_{lc} + \Delta t) \end{array} \right. & \text{if } \lambda_\alpha(t_{lc}) < \lambda_\alpha(t_{lc} + \Delta t) \\ \min \{ \tau | \tau > 0 \text{ and } \eta_\alpha(\tau) + w_\alpha/2 > 0 \} & \text{otherwise} \end{cases} \quad (19)$$

Then the lane change duration is obtained trivially from

$$T_{lc} = \tau_e - \tau_s \quad (20)$$

In total, 1,231 lane changes were investigated, 1,105 of which were suitable to calculate T_{lc} according to Equation 20. In the remaining 126 cases, either τ_s or τ_e were undefined because the corresponding condition was not fulfilled for any $\tau \in [-10, 10]$ within the 20-s environment around the lane change. This can be attributed to vehicle dimension detection errors or vehicle tracking errors, both leading to a trajectory where the vehicle drives on the lane boundary for some time. Figure 8b shows the distribution of the lane-change duration of the examined lane changes. The figure shows that most lane changes take about 3 s (mode value of the distribution), a value found valid for German highways in 1978 (18), but which is substantially different from the one obtained by rule of thumb from the conditional probability density $p(\eta|\tau)$. The mean and standard variation of the distribution are

$$\bar{T}_{lc} = 4.01 \pm 2.31 \text{ s} \quad (21)$$

However, one should be aware that Equation 19 measures the time span where the vehicle occupies two lanes, which only can be taken as a lower bound of the real lane-change duration. Including the preparation and possible postprocessing of a lane change, a value of 5 to 6 s may appear realistic. Since the real beginning of a lane change—the decision for making the lane change—is impossible to measure, and the physical beginning—the moment at which the driver starts to turn the wheel—is very difficult if not impossible to measure, the proposed definition is a good estimator for the lane-change

duration, because it uses well-defined and easily measurable quantities.

Figure 8c shows the conditional probability density of the velocity difference between the leader on the destination lane and the leader on the source lane for different fixed times relative to the lane-changing event. As indicated by the white line, the mean value rises before the lane change by approximately 1 m/s. This indicates that drivers perceive a velocity advantage on the destination lane before performing the lane-changing maneuver and take anticipatory actions.

DISCUSSION AND FUTURE RESEARCH

The availability of the NGSIM data sets spurred considerable research activity, particularly for lane changing, where larger-scale empirical investigations are possible for the first time. Most researchers have used only the positional information, which allows, for example, investigation of the lane-changing rate, the duration of lane changes, the gap acceptance behavior, or the propagation velocity of longitudinal density waves.

The full potential of the data, that is, using the positional information together with that for velocity and acceleration, has not been tapped. This may be because the velocity and acceleration information cannot be used directly since the noise of the positional information is greatly increased by the necessary numerical differentiations. This paper developed a filter to extract more realistic velocity and acceleration information from the positional data. Since the trajectories are comparatively short, the boundary regions were included in the filtered output by reducing the width of the necessary smoothing operations near the boundary. This implies determining the most efficient order of the smoothing and differentiation operations of the filter since they no longer commute, and a wrong order may even lead to a systematic bias.

It is inherently difficult to determine the optimal filter parameters that eliminate most of the noise while retaining the real information. This is particularly crucial for mean-reverting quantities such as the accelerations, where large smoothing time intervals will eventually suppress the whole information. Clearly, further research is necessary to develop more sophisticated, possibly nonlinear, filters.

The velocity and acceleration information of the trajectories can be used in many ways. This work investigated the systematic errors in determining spatial quantities from temporal information, and vice versa. The background is that spatial quantities, such as the gap to the leading vehicle, the density, or the times to collision, usually are estimated by single-vehicle data from stationary detectors, that is, by using temporal information. Use of virtual stationary detectors that are fed with the trajectory data, and simulation of the estimation procedure, allowed quantitative determination of the resulting estimation errors. In addition to the well-known underestimation of the real density of congested traffic, the percentage of critical values of times-to-collision was found to be underestimated by a factor of 2 and more when estimated from single-vehicle data. This is relevant for safety-related applications.

Another application field is empirical tests and parameter calibrations for car-following and lane-changing models. This work showed that before a discretionary lane change, there is a noisy and small, but significant, velocity difference in favor of the target lane. From this it can be concluded that lane-changing decisions are based not only on gaps and velocities but also on velocity differences and, possibly, on accelerations (19).

More generally, the trajectory data allow one to empirically investigate the strategical and tactical actions for preparing or facilitating a lane change (20). Apart from the actions of the lane-changing driver, this includes the actions of the other drivers involved, such as cooperative actions of the follower on the target lane to allow zip-like merging. This is relevant for microscopic simulation software since it turned out to be notoriously difficult to model realistic lane changes, particularly in the case of mandatory changes in congested traffic.

The acceleration information in the data can be used to investigate to what extent the local traffic environment (consisting, e.g., of the next-nearest and further leading vehicles) influences longitudinal driving behavior (20). For example, it has been proposed that driving style is influenced by local velocity variance as determined from few leading vehicles (21).

Finally, the velocity and acceleration information can be used to determine the influence of traffic congestion on the fuel consumption and emissions (15). Since reliable characteristic maps are available for the instantaneous fuel consumption and emission rates of various pollutants as a function of velocity and acceleration, these quantities can now be estimated, for real situations, with unprecedented accuracy.

ACKNOWLEDGMENT

The authors thank FHWA for providing the NGSIM trajectory data used in this study.

REFERENCES

1. *NGSIM: Next Generation Simulation*. FHWA, U.S. Department of Transportation. www.ngsim.fhwa.dot.gov. Accessed May 5, 2007.
2. Skabardonis, A. *Estimating and Validating Models of Microscopic Driver Behavior with Video Data*. Technical report. California Partners for Advanced Transit and Highways, 2005.
3. Lu, X.-Y., and A. Skabardonis. Freeway Traffic Shockwave Analysis: Exploring NGSIM Trajectory Data. Presented at 86th Annual Meeting of the Transportation Research Board, Washington, D.C., 2007.
4. Roess, R. P., and J. M. Ulerio. Analysis of Four Weaving Sections: Implications for Modeling. Presented at 86th Annual Meeting of the Transportation Research Board, Washington, D.C., 2007.
5. Zhang, L., and V. G. Kovvali. Freeway Gap Acceptance Behaviors Based on Vehicle Trajectory Analysis. Presented at 86th Annual Meeting of the Transportation Research Board, Washington, D.C., 2007.
6. Goswami, V., and G. H. Bham. Gap Acceptance Behavior in Mandatory Lane Changes Under Congested and Uncongested Traffic on a Multi-lane Freeway. Presented at 86th Annual Meeting of the Transportation Research Board, Washington, D.C., 2007.
7. Toledo, T., and D. Zohar. Modeling Duration of Lane Changes. In *Transportation Research Record: Journal of the Transportation Research Board, No. 1999*, Transportation Research Board of the National Academies, Washington, D.C., 2007, pp. 71–78.
8. Choudhury, C. F., M. E. Ben-Akiva, T. Toledo, G. Lee, and A. Rao. Modeling Cooperative Lane Changing and Forced Merging Behavior. Presented at 86th Annual Meeting of the Transportation Research Board, Washington, D.C., 2007.
9. Leclercq, L., N. Chiabaut, J. A. Laval, and C. Buisson. Relaxation Phenomenon After Changing Lanes: Experimental Validation with NGSIM Dataset. In *Transportation Research Record: Journal of the Transportation Research Board, No. 1999*, Transportation Research Board of the National Academies, Washington, D.C., 2007, pp. 79–85.
10. Vu, T. T., R. P. Roess, J. M. Ulerio, and E. S. Prassas. Simulation of a Weaving Section. Presented at 86th Annual Meeting of the Transportation Research Board, Washington, D.C., 2007.
11. Jin, W.-L., and L. Li. A Study of First-In First-Out Violation in Freeway Traffic. Presented at 86th Annual Meeting of the Transportation Research Board, Washington, D.C., 2007.

12. Webster, N. A., T. Suzuki, E. Chung, and M. Kuwahara. Tactical Driver Lane Change Model Using Forward Search. Presented at 86th Annual Meeting of the Transportation Research Board, Washington, D.C., 2007.
13. Alecsandru, C., and S. Ishak. Accounting for Random Driving Behavior and Nonlinearity of Backward Wave Speeds in the Cell Transmission Model. Presented at 86th Annual Meeting of the Transportation Research Board, Washington, D.C., 2007.
14. Kesting, A., and M. Treiber. Calibrating Car-Following Models Using Trajectory Data: Methodological Study. In *Transportation Research Record: Journal of the Transportation Research Board, No. 2088*, Transportation Research Board of the National Academies, Washington, D.C., 2008, pp. 148–156.
15. Treiber, M., A. Kesting, and C. Thiemann. How Much Does Traffic Congestion Increase Fuel Consumption and Emissions? Applying a Fuel Consumption Model to NGSIM Trajectory Data. Presented at 87th Annual Meeting of the Transportation Research Board, Washington, D.C., 2008.
16. Hirst, S., and R. Graham. The Format and Presentation of Collision Warnings. In *Ergonomics and Safety of Intelligent Driver Interfaces* (Y. Noy, ed.), Lawrence Erlbaum Associates, Mahwah, N.J., 1997.
17. Minderhoud, M. M., and P. H. L. Bovy. Extended Time-to-Collision Measures for Road Traffic Safety Assessment. *Accident Analysis and Prevention*, Vol. 33, 2001, pp. 89–97.
18. Sparmann, U. Spurwechselforgänge auf zweispurigen BAB-Richtungsfahrbahnen. *Forschung Straßenbau und Straßenverkehrstechnik*, Vol. 263, 1978.
19. Treiber, M., A. Kesting, and D. Helbing. Delays, Inaccuracies and Anticipation in Microscopic Traffic Models. *Physica A*, Vol. 360, 2006, pp. 71–88.
20. Kesting, A., M. Treiber, and D. Helbing. General Lane-Changing Model MOBIL for Car-Following Models. In *Transportation Research Record: Journal of the Transportation Research Board, No. 1999*, Transportation Research Board of the National Academies, Washington, D.C., 2007, pp. 86–94.
21. Treiber, M., A. Kesting, and D. Helbing. Understanding Widely Scattered Traffic Flows, the Capacity Drop, and Platoons as Effects of Variance-Driven Time Gaps. *Physical Review E*, Vol. 74, 2006, p. 016123.

The Traffic Flow Theory and Characteristics Committee sponsored publication of this paper.